Robotica (2014) volume 32, pp. 953–966. © Cambridge University Press 2013
doi:10.1017/S0263574713001112

Some geometric, kinematic, and dynamic considerations on Stewart-Gough platforms with singularity analysis

A. Saide Sarıgül†,* and Burcu Güneri‡

†*Department of Mechanical Engineering, Faculty of Engineering, Dokuz Eylül University, İzmir, Turkey*
‡*İzmir Refinery, Turkish Petroleum Refineries Co., İzmir, Turkey*

(Accepted October 29, 2013. First published online: December 13, 2013)

SUMMARY
In this study, some geometric, kinematic, and dynamic aspects of the design of a Stewart-Gough platform are examined. The focus of the analyses is on a particular Stewart-Gough platform that we have constructed. The analysis begins with workspace simulations for different moving platform orientations. The computations extend to a parametric study of some geometric and kinematic constraints: Joint angle, rotation angle, and limb length. Actuator force is another parameter considered; and the triple relationship between workspace, joint angle, and actuator force is discussed. Parametric analyses are culminated with a brief discussion of the real design parameters.

KEYWORDS: Parallel manipulator; Stewart-Gough platform; Hexapod; Actuator force; Workspace; Singularity.

1. Introduction

Manipulators have wide range of different applications and this makes them very important in the technological world. The studies have started with serial manipulators; continued with parallel manipulators; and the combination of both, hybrid ones. Serial manipulators have the advantage of being able to achieve high velocities and acceleration because the end-effector moves generally faster than the actuated links. Also, they have larger workspace than parallel manipulators. However, they are not very energy efficient because each actuated link also has to carry all the subsequent links and their actuators. Parallel manipulators have the advantages of accuracy, high speed, stiffness, and also greater load-to-weight ratio. Because each actuated leg carries only a part of payload, the robot can handle heavy loads. However, reduced workspace, difficult mechanical design, more complex direct kinematics, and control algorithms are disadvantages of parallel manipulators. Parallel manipulators have been very popular especially in the last two decades and many papers have been published on different aspects or types of them. One of the initial comprehensive studies is that presented by Fichter[1] on the theoretical and practical considerations of a Stewart-Gough platform-based manipulator.

A hybrid type manipulation system is a combination of closed-chain and open-chain mechanisms or it is a sequence of parallel manipulators. The hybrid manipulators overcome the disadvantage of limited workspace of parallel manipulators. Hybrid manipulators have the advantages of both serial and parallel ones such as high rigidity and wide workspace.

Workspace analysis of manipulators is compulsory in order to design a trajectory for the desired task.[2,3] Parallel robots' having limited workspace makes this analysis more important and more necessary. Therefore, workspace phenomenon has been the center of attraction; and different methods for the calculation and broadening of the workspace have been developed by many researchers.[4–26] Another subject that the researches are concentrated on is singularity. Singularity-free path planning is required for the controlled motion of parallel manipulators.[27–29] These studies are also integrated

* Corresponding author. E-mail: saide.sarigul@deu.edu.tr

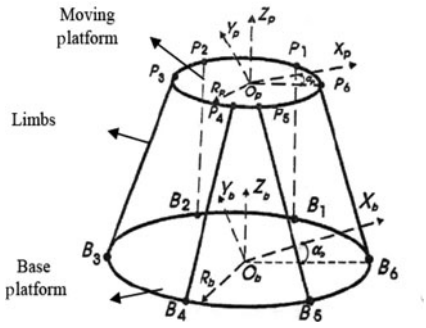

Fig. 1. A simple model of Stewart-Gough platform.

with the workspace concept due to the objective of obtaining singularity-free workspace[30–34] and with an optimal design.[35–39] Another requirement to be able to have an optimal design is monitoring the forces during the motion.[40,41]

Due to the technological requirements, still there are many subjects to discover about the design of parallel manipulators. There are many kinematic and geometric parameters affecting the workspace and actuator forces. A workspace analysis, including singularity detection and force monitoring, is capable of determining whether the robot can do the given task or not. Present study is mainly devoted to examine the design parameters of Stewart-Gough platforms on a singularity-free workspace basis. Tests were conducted on a realized platform that provided fixed variables of the parametric analyses.[42]

In the paper, firstly, the computed workspace of the manipulator is presented and the effect of moving platform's orientation on the shape and dimension of the workspace is analyzed. Then the influences of the constraints, joint angle, joint rotation angle, and limb length on the dimension of a representative plane, workplane, of the workspace are examined. This analysis exposes the constraint that has priority in limiting the prescribed motion. Another analysis is a combined one, putting forward the workspace-actuator force-joint angle relationship and the necessity of an optimal design. Parametric analyses include a brief discussion on the real design parameters of the Stewart-Gough platform.

In order to provide a singularity-free motion to the manipulator, all analyses were conducted under the control of a trajectory planning code. Therefore, final section is composed of an overview with some results of the singularity inquiry on the basis of the condition number.

2. Modeling and Inverse Kinematic Analysis

Stewart-Gough platform is a kind of hexapod, a parallel manipulator with six limbs and six degrees of freedom. This spatial manipulator has identical limbs with spherical–prismatic–spherical (SPS) joints. Each limb of the manipulator contains one passive degree of freedom.[43] Fig. 1 shows a simple model of the Stewart-Gough platform with the angles defining joint locations and other notifications used in the formulae. If both platforms of the manipulator are divided into three parts by imaginary axes 120° apart, spherical joints are located on the base and moving platforms at the points B_i and P_i ($i = 1, 2, \ldots, 6$) with joint angles α_b and α_p from the related axes, respectively. R_b and R_p are radii of the circles on which spherical joints are located on the base and moving platforms, respectively.

If $\boldsymbol{u}$, $\boldsymbol{v}$, and $\boldsymbol{w}$ are the mutually orthogonal basis vectors of the reference frame F_p fixed to the moving platform P, rotation matrix ${}^bR_p$ defining coordinate system of the moving platform with respect to that of the base platform is given as

$$ {}^b\boldsymbol{R}_p = \begin{bmatrix} u_x & v_x & w_x \\ u_y & v_y & w_y \\ u_z & v_z & w_z \end{bmatrix}. \tag{1} $$

Here, the symbols x, y, z represent the coordinate axes of the reference frame F_b fixed to the base platform B and $u_x, u_y, \ldots, w_z$ are the components of the basis vectors of the frame F_p that are expressed in the frame F_b.

https://doi.org/10.1017/S0263574713001112 Published online by Cambridge University Press

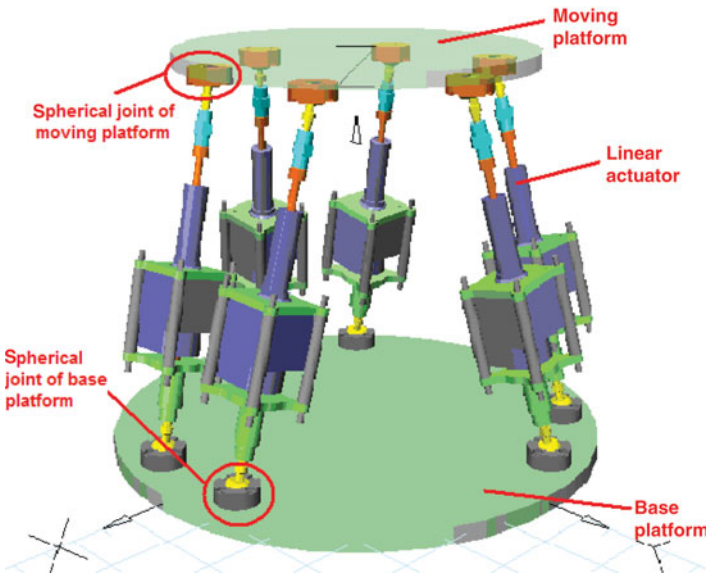

Fig. 2. (Colour online) Solid model of the Stewart-Gough platform.

Limb vector can be found by the loop-closure equation (Fig. 1)

$$\boldsymbol{l_i} = \boldsymbol{d} + {}^{b}\boldsymbol{R}_p \boldsymbol{p_i} - \boldsymbol{b_i} \qquad i = 1, 2, \ldots, 6, \tag{2}$$

where $\boldsymbol{l_i} = L_i \boldsymbol{s_i} = L_i[s_{ix}\ s_{iy}\ s_{iz}]^T$, $\boldsymbol{d} = [d_x\ d_y\ d_z]^T$, $\boldsymbol{b}_i = [b_{ix}\ b_{iy}\ b_{iz}]^T$, $\boldsymbol{p}_i = [p_{iu}\ p_{iv}\ p_{iw}]^T$. L_i is the length of the ith limb, $\boldsymbol{s_i}$ is the unit vector along the ith limb, $\boldsymbol{d}$ is the position vector from the center of the base platform to the center of the moving platform, and $\boldsymbol{b_i}$ and $\boldsymbol{p_i}$ are radius vectors of the respective platforms.

All parts of the manipulator were designed by using a solid modeling program. In the design process, relative motions and joint constraints were defined. Then the parts were combined together to form the whole mechanism. The solid model of the robot used for simulations is shown in Fig. 2. In the determination of actuator forces, limb weights were taken into account whereas inertias were not considered because of the low working velocities. Performing necessary computations and simulations in order to ensure that the actuator forces are in allowable limits and dimension of the workspace is large enough to accomplish the given task, the real manipulator was produced. The Stewart-Gough platform with $R_b = 0.149$ m and $R_p = 0.1$ m is shown in Fig. 3.

3. Workspace Analysis

Parallel manipulators have complex kinematic equations and their forward kinematics is even more tedious. Therefore, although the workspace determination is a challenging problem, due to the comparatively restricted workspace of parallel manipulators, this computation and trajectory planning become urgent. Eventually, some algorithms have to be developed to calculate the workspace, and some attempts should be undertaken to expand the machining range of work-piece if necessary.

There are some geometric and kinematic constraints affecting the workspace of a parallel manipulator. General dimensions and joint angles are geometric constraints whereas joint rotation angle, limb length, and limb interference limitations are kinematic constraints. Joint angles describe the joint positions with respect to the coordinate axes on the platforms. Joint rotation angles define configuration of limbs with respect to the normal vectors of platforms. In this study, the effect of moving platform orientation, joint angle, joint rotation angle, and limb length limitations on the workspace are examined. On the other hand, the relationship between the workspace–joint angle–actuator force is also considered. This combined analysis brings a vision on evaluating kinematic and kinetic effects together in terms of workspace.

https://doi.org/10.1017/S0263574713001112 Published online by Cambridge University Press

Fig. 3. (Colour online) Produced Stewart-Gough platform.

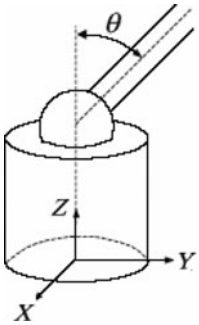

Fig. 4. Joint rotation angle θ.

3.1. Workspace calculations

There are different geometrical or analytical methods in literature in order to calculate the workspace. In this study, a code computing "constant orientation workspace" was developed on the basis of the algorithm in reference.[44] The method depends on finding the boundary curves on each horizontal plane and then combining them to form a boundary surface of the workspace. The computer code performs inverse kinematic analysis and controls limiting parameters for each spatial point considered. For this purpose, Eqs. (1) and (2) are used with the following constraint equations:[20]

$$L_{\min} \leq L_i \leq L_{\max} \tag{3a}$$

$$\theta_{pi} = cos^{-1}(-\boldsymbol{l_i} \cdot {}^{\boldsymbol{b}}\boldsymbol{R_p}\, \boldsymbol{n_{pi}}/|\boldsymbol{l_i}|) \leq \theta_{p\max} \tag{3b}$$

$$\theta_{bi} = cos^{-1}(\boldsymbol{l_i} \cdot \boldsymbol{n_{bi}}/|\boldsymbol{l_i}|) \leq \theta_{b\max} \tag{3c}$$

Here, $L_{\min}$ and $L_{\max}$ denote the minimum and maximum limb length limitations, respectively. θ is the joint rotation angle measured from normal of a platform to the limb as shown in Fig. 4. $\theta_{p\max}$ and $\theta_{b\max}$ are the maximum rotation angle limits for the joints mounted on the moving and base platforms, respectively. $\boldsymbol{n_{pi}}$ and $\boldsymbol{n_{bi}}$ are the unit vectors normal to the moving and base platforms, given as $[0\ 0{-}1]^T$ and $[0\ 0\ 1]^T$ in respective coordinate systems (Fig. 5).

https://doi.org/10.1017/S0263574713001112 Published online by Cambridge University Press

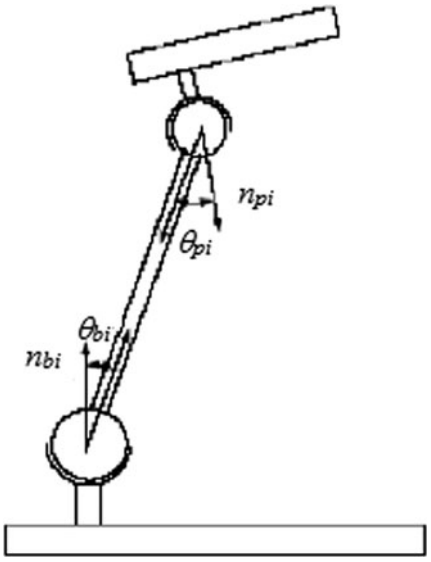

Fig. 5. Configuration of a limb.

3.2. Workspace analysis for different orientations of the moving platform

The workspace of the Stewart-Gough platform was established for different orientations of the moving platform. Orientations were provided by setting Euler angles β_x and β_y about fixed x and y axes of the base platform. The effect of β_z angle is insignificant in our moving platform, because the tool attached has circular symmetry about the normal axis of the platform and it operates with a spinning motion about that axis. Rotation matrices of the moving platform are

$$R\left(y, \beta_y\right) = \begin{bmatrix} cos\beta_y & 0 & sin\beta_y \\ 0 & 1 & 0 \\ -sin\beta_y & 0 & cos\beta_y \end{bmatrix}, \tag{4}$$

$$R\left(x, \beta_x\right) = \begin{bmatrix} 1 & 0 & 0 \\ 0 & cos\beta_x & -sin\beta_x \\ 0 & sin\beta_x & cos\beta_x \end{bmatrix}. \tag{5}$$

The sequence of Euler angles is selected as β_x and β_y. The resultant rotation matrix is obtained by the premultiplication of the basic rotation matrices[43]

$$R = R(y, \beta_y)\, R(x, \beta_x) \tag{6}$$

resulting,

$$R = \begin{bmatrix} cos\beta_y & sin\beta_y sin\beta_x & sin\beta_y cos\beta_x \\ 0 & cos\beta_x & -sin\beta_x \\ -sin\beta_y & cos\beta_y sin\beta_x & cos\beta_y cos\beta_x \end{bmatrix}. \tag{7}$$

The workspace of the manipulator for different orientations of moving platform is presented in Fig. 6. The isometric views of the workspace extends from $z = 0.23$ m to $z = 0.27$ m, the maximum height. Here, z is the distance between center points of the planes where the centers of the spherical joints lie. The computations were performed with $\Delta z = 0.001$ m intervals.

As seen in Fig. 6, the effect of orientation angle β is to reduce the workspace. In addition, combined orientation in two axes results in the lowest workspace volume. On the other hand, the symmetry of workspace changes with regard to the direction of rotation. For horizontal position of the moving platform, workspace is symmetric in radial direction. Orientation about x-direction provides symmetry about an inclined axis whereas orientation about y-direction leads to symmetry about central horizontal axis. Orientation in both directions gives rise to inclination of the symmetry

https://doi.org/10.1017/S0263574713001112 Published online by Cambridge University Press

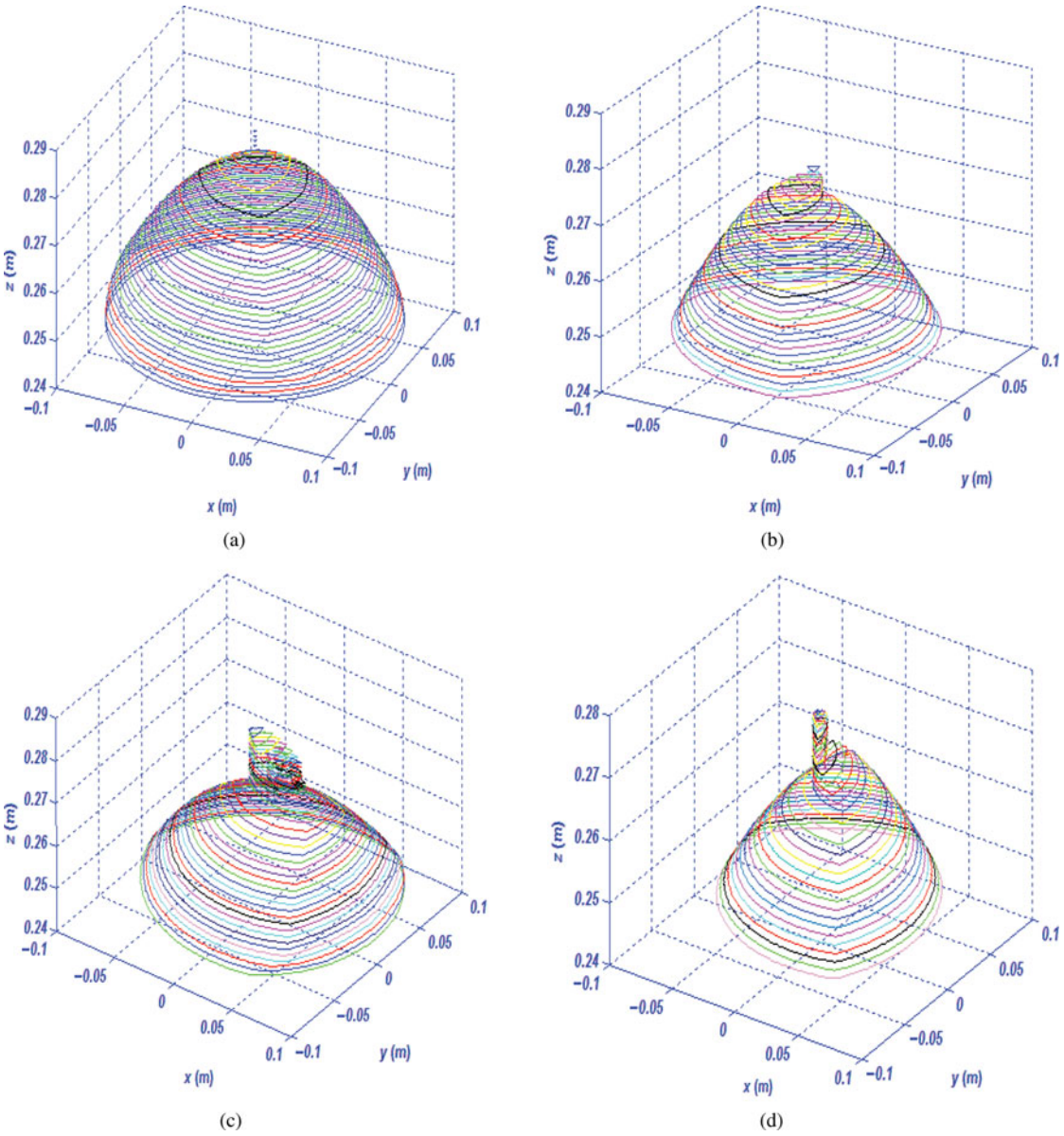

Fig. 6. (Colour online) Workspace of the Stewart-Gough platform for different orientations: (a) $\beta_x = 0^\circ$, $\beta_y = 0^\circ$; (b) $\beta_x = 5^\circ$, $\beta_y = 0^\circ$; (c) $\beta_x = 0^\circ$, $\beta_y = 5^\circ$; (d) $\beta_x = 5^\circ$, $\beta_y = 5^\circ$.

axis. Orientation angles cause rapid decrease in the workspace at higher levels. While moving on these locations, actuator forces increase and motion ability of the robot ceases.

3.3. Parametric effects on workspace

In this analysis, the relations between three constraints and workspace are examined. These constraints are joint angle, maximum rotation angle, and limb length. A specific plane ($z = 0.235$ m) of the workspace is selected as the representative workplane. The workplane area is evaluated by numerical integration. The effects of geometric and kinematic constraints on the size of the workplane are examined for the four orientations of the moving platform. In each case, one parameter is changed whereas the other two are kept constant.

3.3.1. Effect of joint angle. Joint angles (α) define the location of joints on the platforms. The effect is considered by changing joint angles on the moving platform. The base platform's joint angles are kept constant as $\alpha_b = 15^\circ$ for all analyses, only for convenience. The boundaries of the curves defining the maximum areas reached by the manipulator are determined for eight different joint angles

https://doi.org/10.1017/S0263574713001112 Published online by Cambridge University Press

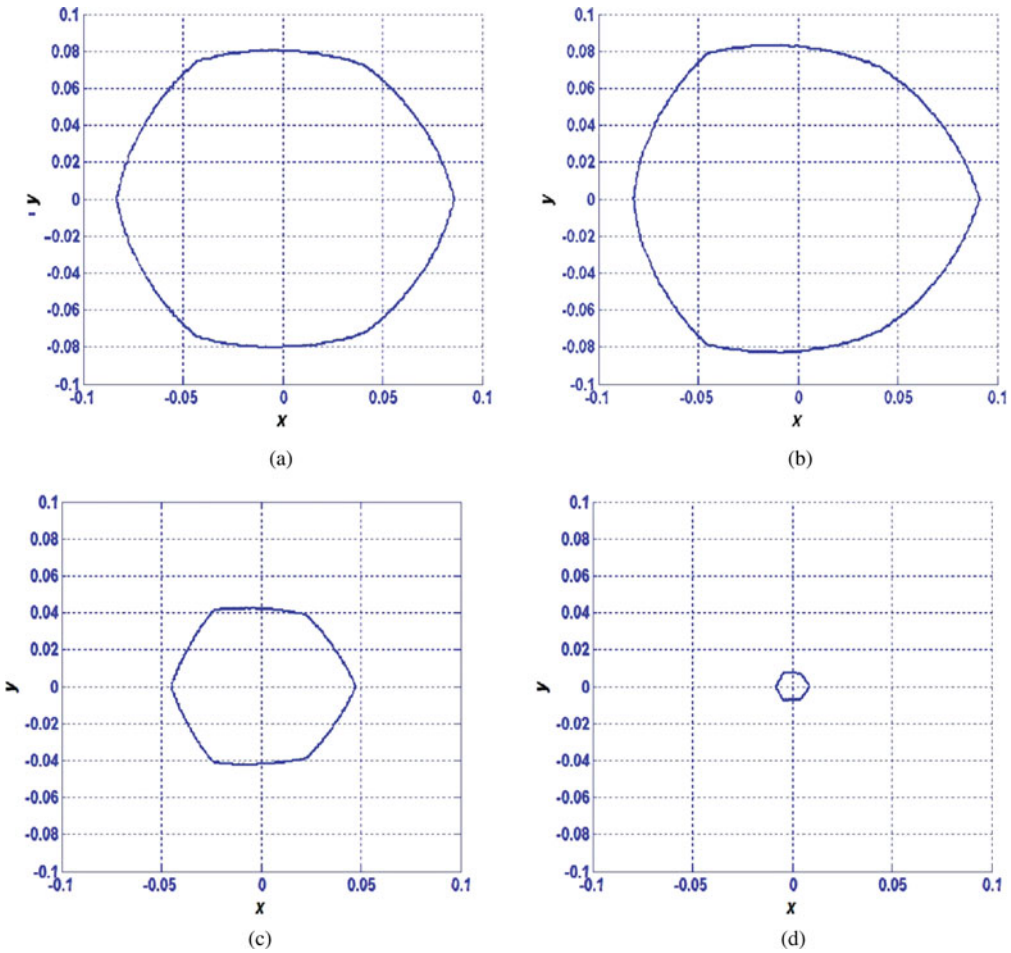

Fig. 7. (Colour online) Workplane boundaries for $\beta_x = 0°$, $\beta_y = 0°$: (a) $\alpha_p = 10°$; (b) $\alpha_p = 15°$; (c) $\alpha_p = 50°$; (d) $\alpha_p = 70°$.

($\alpha_p = 10°, 15°, 25°, 30°, 40°, 50°, 60°, 70°$), including the real one (30°). The workplane boundary curves are presented in Fig. 7 for the horizontal position and four of the joint angles. The workplane area is calculated numerically by using Green's theorem.

Fig. 8 shows joint angle–workplane area relationship including the orientation of the moving platform. It is clear that as the moving platform's joint angle becomes closer to 15° , base platform's joint angle, the workplane area continuously increases. However, since the equality of joint angles causes to singularity, this configuration is not recommended.[44] The gain in the workplane area is almost linear between 25° and 45° and this trend decelerates below 25°. The present joint angle (30°) is suitable for reaching large workspace without approaching singularity.

3.3.2. Effect of maximum rotation angle. Joint rotation angles (θ) are tilt angles of spherical joints. The analysis includes five different angles $\theta_{p\max} = \theta_{b\max} = 15°, 20°, 25°, 30°, 40°$ and the real limit 45°. Fig. 9 shows maximum rotation angle–workplane variation with the moving platform's orientation. The orientation has an obvious workplane decreasing effect. The workplane area for the horizontal position makes a peak at 30°, and continues steadily. Beyond this angle, workplane cannot increase since limb lengths reach their upper constraint $L_{\max}$. However for the other orientations, the workplane becomes constant after 40°. Therefore, joints may be chosen by taking limb length limitations into account for a feasible design. An angle limitation of 45° for the manufactured Stewart-Gough platform is safely large enough to be able to widen workplane if the limb length would be increased.

3.3.3. Effect of limb length. Limb length limitations for defining the workspace include maximum and minimum limb lengths, or maximum extension ($\Delta L_{\max}$) of the limbs. In this analysis, five different

https://doi.org/10.1017/S0263574713001112 Published online by Cambridge University Press

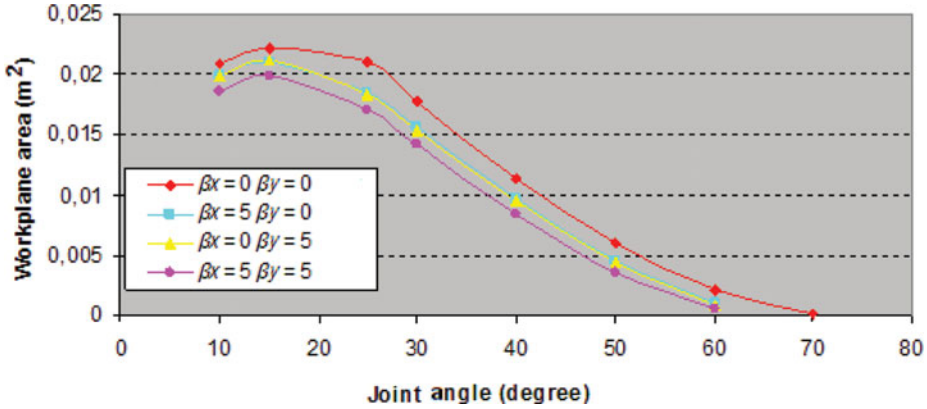

Fig. 8. (Colour online) The variation of workplane with joint angle and orientation.

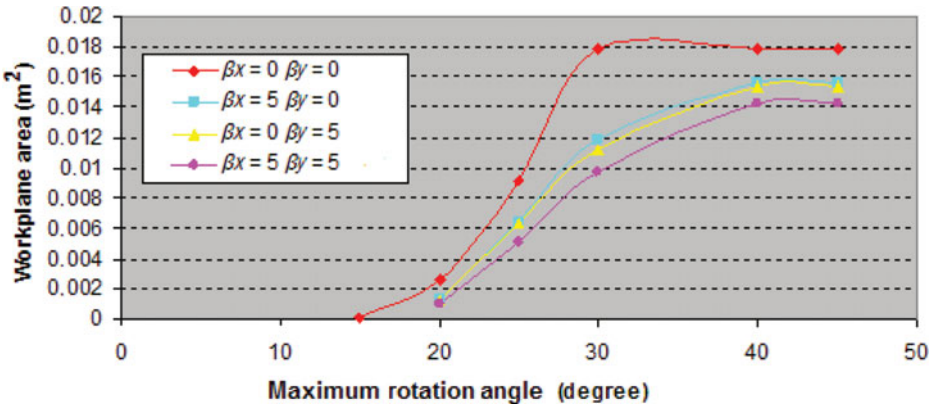

Fig. 9. (Colour online) The variation of workplane with maximum rotation angle and orientation.

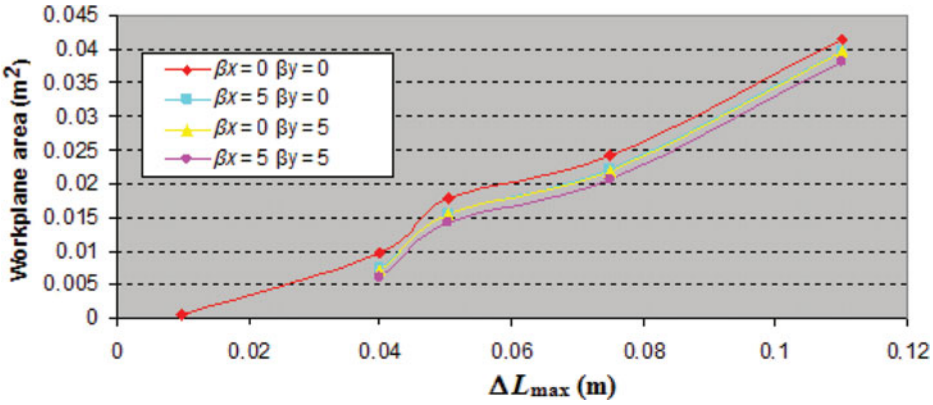

Fig. 10. (Colour online) The variation of workplane with limb length limit and orientation.

motion ranges of the actuators are $\Delta L_{\max} = 0.01$ m, 0.04 m, 0.050464 m, 0.075 m, 0.11 m where 0.050464 m is the real limb limitation. The results are presented in Fig. 10. The increase in the moving range of actuators widens the workplane almost linearly. When the platform is orientated, motion is restricted for lower limb limits. The real limit is high enough letting the oriented motion.

3.4. Workspace–joint angle–actuator force relationship

Workspace–joint angle–actuator force relationship of the manipulator is a combination of geometric, kinematic, and kinetic factors. The analysis is performed by using the results of five different design simulations where moving platform's joint angle is the free variable with $\alpha_p = 20^\circ, 25^\circ, 30^\circ, 36^\circ$, and

https://doi.org/10.1017/S0263574713001112 Published online by Cambridge University Press

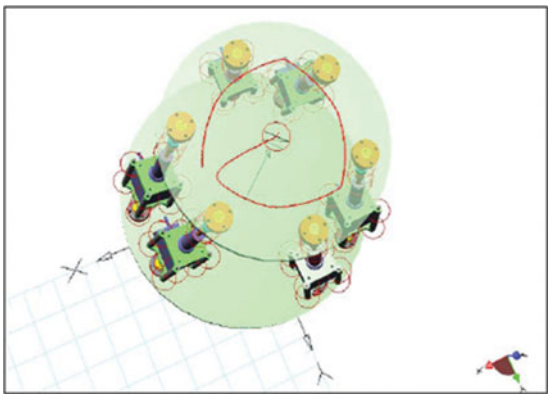

Fig. 11. (Colour online) 3-D view of the simulation model for joint angle $\alpha_p = 30^\circ$ after completing the trajectory.

44°. Base platform's joint angle is kept constant as $\alpha_b = 15^\circ$. The areas of workplanes representing workspace are computed at $z = 0.257$ m plane that lies approximately at one-third of the moving platform's vertical range.

In the analysis, the weights of the elements forming the manipulator are taken into consideration. Inertia forces are not included since velocities of the moving parts are generally low and constant. Actuator forces for each α_p angle are determined by using the following procedure:

- The recorded coordinates of the points on the boundary curve of the computed workplane such as presented in Fig. 7 are transferred to the simulation program as input of the prescribed motion. The manipulator is adjusted to complete the pursuit of the workplane boundary in 360 s. The three-dimensional view of the model for $\alpha_p = 30^\circ$ after completing the indicated trajectory is given in Fig. 11.
- In the first set of simulations, force constraint is selected and set to zero for all the actuators. Actuator length data is saved.
- Before the second set of simulations, the prescribed motion input is disabled and actuator length constraint is selected. Second simulation set is launched with the recorded actuator length data. Forces on the actuators are recorded.

The variation of dynamic actuator forces changing from time to time is presented in Fig. 12.

Each application for different joint angles brings out similar trajectories and force variations. Their numerical compositions are presented in Figs. 13 and 14 in terms of workplane area and maximum actuator force, respectively. Fig. 13 is a reproduction of Fig. 8 only for a different horizontal plane. Fig. 14 shows the increase in the forces for more inclined limbs as the manipulator reaches further points, enlarging workplane boundaries.

It is clear that the maximum actuator force is for the joint angle giving the largest workplane area. However, as the joint positions of the two platforms become closer the gain in the area gets smaller whereas the increase in the force is really significant. Strictly speaking, an optimization study is required for a definite determination of joint angle, the most suitable to the specific application. However, the present joint angle $\alpha_p = 30^\circ$ may be considered as a fair choice in terms of both workplane and actuator force.

4. Singularity Analysis

As it is known, singularity is an important limitation for motion of robots in terms of accomplishing the desired task. In a singular configuration, the manipulator may lose or gain extra degrees of freedom, becomes uncontrollable, or forces on the actuators may diverge to infinity, which results in the breakage of actuators. If singularity analysis of a manipulator is performed before giving a task, the robot's ability in accomplishing the prescribed motion can be tested and any undesirable situation can be prevented.

https://doi.org/10.1017/S0263574713001112 Published online by Cambridge University Press

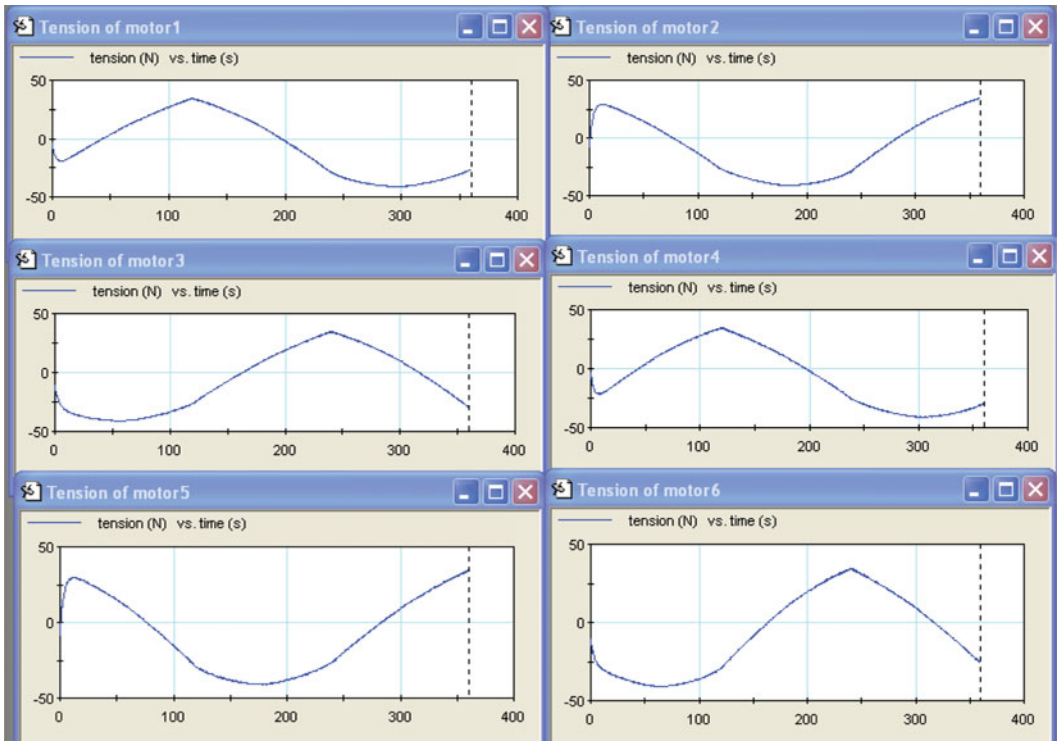

Fig. 12. (Colour online) Variation of actuator forces on the pursuit of boundary trajectory.

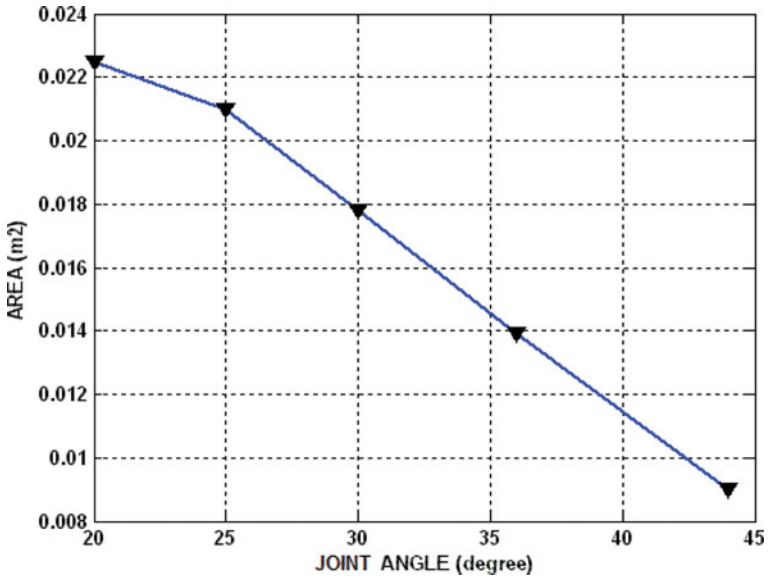

Fig. 13. (Colour online) Workplane areas for different joint angles of the moving platform.

4.1. Jacobian matrix

If the position of joints is denoted by a vector $\boldsymbol{q}$ and the location of the moving platform is described by a vector $\boldsymbol{x}$, these motions are constrained in the loop-closure equation

$$\boldsymbol{f}(\boldsymbol{x}, \boldsymbol{q}) = \boldsymbol{0}, \tag{8}$$

https://doi.org/10.1017/S0263574713001112 Published online by Cambridge University Press

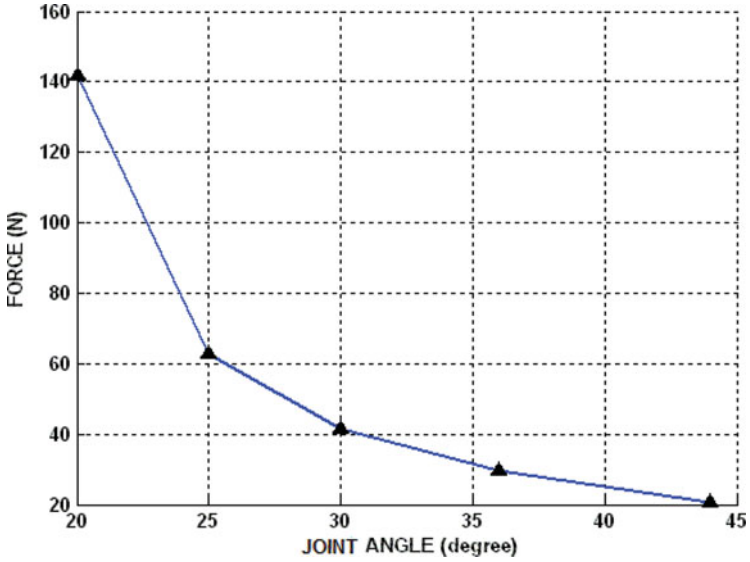

Fig. 14. (Colour online) Maximum actuator forces for different joint angles of the moving platform.

where $\boldsymbol{f}$ is an n-dimensional implicit function of $\boldsymbol{q}$ and $\boldsymbol{x}$. n is the degree of freedom of the manipulator. Differentiating Eq. (8) with respect to time,

$$\boldsymbol{J}_x d\boldsymbol{x}/dt = \boldsymbol{J}_q d_q/dt, \tag{9}$$

two separate Jacobian matrices of the parallel manipulator are obtained. Here,

$$\boldsymbol{J}_x = \partial \boldsymbol{f}/\partial \boldsymbol{x}, \tag{10}$$

$$\boldsymbol{J}_q = -\partial \boldsymbol{f}/\partial \boldsymbol{q}. \tag{11}$$

The overall Jacobian matrix is given as

$$\boldsymbol{J} = (\boldsymbol{J}_q)^{-1} \boldsymbol{J}_x. \tag{12}$$

The singular configurations may be examined mathematically by the singularity of the Jacobian matrices. Singularity of $\boldsymbol{J}_q$ is "inverse kinematic singularity" and manipulator loses one or more degrees of freedom. $\boldsymbol{J}_x$ singularity is "direct kinematic singularity" and manipulator gains one or more degrees of freedom. "Combined singularity" occurs when both $\boldsymbol{J}_q$ and $\boldsymbol{J}_x$ are singular.[43]

Jacobian matrices of the Stewart-Gough platform are obtained by the derivation of the loop-closure Eq. (2) with respect to time:

$$\boldsymbol{J}_x = \begin{bmatrix} \boldsymbol{s}_1^T & \boldsymbol{a}_1^T \\ \boldsymbol{s}_2^T & \boldsymbol{a}_2^T \\ \vdots & \vdots \\ \boldsymbol{s}_6^T & \boldsymbol{a}_6^T \end{bmatrix}, \tag{13}$$

$$\boldsymbol{J}_q = \boldsymbol{I} \ (6 \times 6 \text{ identity matrix}).$$

Here, $\boldsymbol{a}_i = {}^b\boldsymbol{R}_p \boldsymbol{p}_i \times \boldsymbol{s}_i$. Since $\boldsymbol{J}_q$ is an identity matrix; only "direct kinematic singularity" may present within the workspace of a Stewart-Gough platform.

In the present study, a computer code checking the singularity of the Jacobian matrix $\boldsymbol{J}_x$ in Eq. (13) was written and the determinant of $\boldsymbol{J}_x$ for different points in the workspace was computed. Except theoretically known configurations, no singularity for the present analyses and also other test trajectories, such as a line, cardoid, and spherical surface, was approached.

https://doi.org/10.1017/S0263574713001112 Published online by Cambridge University Press

Table I. Condition numbers for the moving platform orientation, $\beta_x = 0^\circ$, $\beta_y = 0^\circ$.

Plane level z (m)	First point condition number	Last point condition number	Minimum condition number	Maximum condition number
0.210	–	–	–	–
0.220	57.0480	70.4531	57.0480	70.5771
0.230	59.6411	68.9893	59.6411	69.0905
0.240	62.2341	67.9158	62.2341	67.9930
0.250	64.8272	67.2726	64.8272	67.2726
0.260	67.4203	67.6089	67.4203	67.6089

4.2. Condition number

Since elements of Jacobian matrix do not have uniform dimensions, attention is necessary in its manipulation for the singularity analysis. A non-dimensional measure for the singularity of manipulators having one type of joints is "condition number."[43] Condition number κ ($\boldsymbol{J}$) of the Jacobian matrix may be formulated as:

$$\kappa(\boldsymbol{J}) = \|\boldsymbol{J}\| \, \|\boldsymbol{J}^{-1}\|, \tag{14}$$

where $\| \, . \, \|$denotes the norm of the matrix.

Minimum possible value of the condition number is "1" and small values indicate well-conditioning. Large values indicate ill-conditioning and at a singular configuration, condition number becomes infinite. For a non-singular configuration of the robot, condition number must be lower than a limit value, κ_{lim}.[45] Since during a motion condition number generally lies in an interval, the limit for the condition number can be chosen by multiplying the upper interval bound with a safety factor. This safety factor may be assumed between 1.5 and 4. Taking large condition number limits causes more rough results and may lead researcher to lose some of the singular points.

All of the previous analyses were conducted also by the computation of condition numbers for singularity inquiry. Condition numbers calculated at different planes for the parallel position of the platform with its real parameters are shown in Table 1. The four of condition numbers among the many ones computed for regularly placed points within each workplane boundary are presented. These are the first point–last point and the minimum–maximum condition numbers. The first point and last point condition numbers correspond to the beginning and end of the trajectory. These four values are sufficient to detect the behavior of the condition numbers in a prescribed motion.[45] The empty row in Table 1 indicates a discontinuous workplane because only continuous workplanes reachable for the manipulator are considered. Although, in general, condition numbers tend to increase with the manipulator's movement to further points in the workspace, they are small enough implying no singularity.

Fig. 15 shows the variation of maximum condition numbers for different orientations of moving platform of the examined manipulator. The lowest condition numbers are obtained for the horizontal position since motion ability is the highest for this configuration and the robot moves without extra force. On the other hand, rotations about only one axis expose larger results than that about both axes. This phenomenon may be expressed by the dimension of the workspace. As demonstrated through the paper, the workspace is the smallest for the combined orientation case and the lowest numbers are computed among the three moving platform-oriented cases. Another feature is the reduction in condition numbers with height, in parallel to workplane area.

5. Conclusions

The effects of some geometric and kinematic design parameters were studied for a realized Stewart-Gough platform with regard to workspace phenomenon with singularity inquiry. The parameters were joint angle, rotation angle, and limb length, and the analyses included different orientations of the moving platform. On the other hand, the cross-connection among the workspace, joint angle, and actuator force was examined. The study was performed through the codes developed to solve inverse kinematic equations, and also simulations by solid modeling and analysis programs.

https://doi.org/10.1017/S0263574713001112 Published online by Cambridge University Press

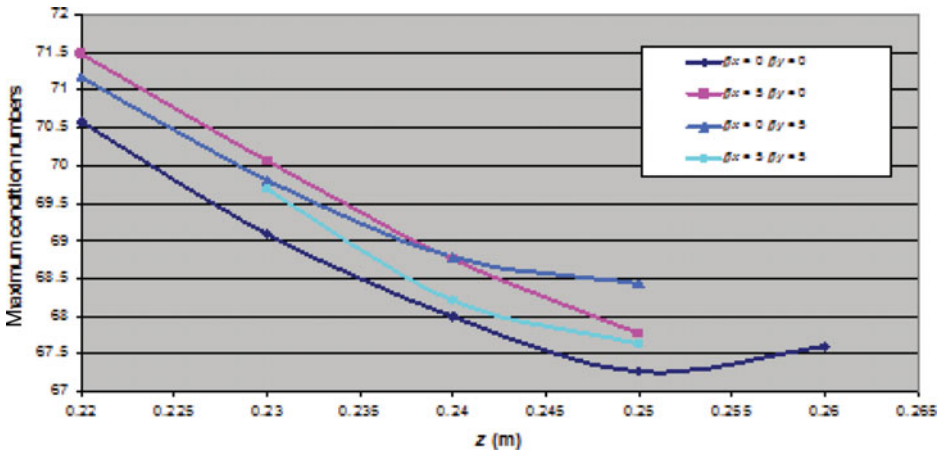

Fig. 15. (Colour online) Maximum condition numbers for different orientations of the moving platform.

In all cases examined, maximum workspace is attained for the parallel orientation of the moving platform. The limb length limitation appears as the most prominent constraint from the point of view of the workspace. On the other hand, the increase in the other constraint, rotation angle limit, affects the workspace in a positive manner on a specific range. From the point of view of the third constraint, joint angle, the closer the angles of base and moving platforms, the larger the workspace. However for this case, actuator forces highly increase and singularity problem arises. An optimization study may provide the most suitable value of joint angle in both aspects: workspace and actuator force.

Singularity checks based on both Jacobian matrix and condition number accompanied to all analyses. Any singularity phenomenon was not detected, and all the foregoing analyses exposed that design parameters chosen for the prototype model are fairly good and the constructed Stewart-Gough platform is very effective and stable.

Acknowledgements

Authors present their special thanks to The Scientific and Technological Research Council of Turkey (TÜBİTAK) for giving support to the research project with project number 104M373.

References

1. E. F. Fichter, "A Stewart platform based manipulator: General theory and practical considerations," *Int. J. Robot. Res.* **5**(2), 157–182 (1986).
2. M. Ceccarelli, "A formulation for the workspace boundary of general N-revolute manipulators," *Mech. Mach. Theor.* **31**(5), 637–646 (1996).
3. G. S. Chirikjian and I. Ebert-Uphoff, "Numerical convolution on the Euclidean group with applications to workspace generation," *IEEE Trans. Robot. Autom.* **14**(1), 123–136 (1998).
4. H. Asada and K. Youcef-Toumi, "Analysis and design of a direct-drive arm with a five-bar-link parallel drive mechanism," *ASME J. Dyn. Syst. Meas. Control* **106**(3), 225–230 (1984).
5. D. C. H. Yang and T. W. Lee, "Feasibility study of a platform type of robot manipulators from a kinematic viewpoint," *ASME J. Mech. Transmissions Autom. Des.* **106**, 191–198 (1984).
6. A. Bajpai and B. Roth, "Workspace and mobility of a closed-loop manipulator," *Int. J. Robot. Res.* **5**(2), 131–142 (1986).
7. K. M. Lee and D. K. Shah, "Kinematic analysis of a three-degree-of-freedom in-parallel actuated manipulator," *IEEE J. Robot. Autom.* **14**(3), 354–360 (1988).
8. C. C. Nguyen and F. J. Pooran, *Kinematic Analysis and Workspace Determination of a 6 Dof CKCM Robot End-Effector* (Elsevier, Amsterdam, 1989).
9. C. Gosselin, "Determination of a workspace of 6-DOF parallel manipulators," *ASME J. Mech. Des.* **112**, 331–336 (1990).
10. V. Kumar, "Characterization of workspaces of parallel manipulators," *ASME J. Mech. Des.* **114**, 368–375 (1992).
11. J. P. Merlet, "Determination of the workspace of a parallel manipulator for a fixed orientation," *Mech. Mach. Theor.* **29**(8), 1099–1110 (1994).
12. J. P. Merlet, "Trajectory verification in the workspace for parallel manipulators," *Int. J. Robot. Res.* **13**(4), 326–333 (1994).

https://doi.org/10.1017/S0263574713001112 Published online by Cambridge University Press

13. Z. Ji, "Workspace analysis of Stewart platforms via vertex space," *J. Robotic Syst.* **11**(7), 631–639 (1994).
14. C. Luh, F. Adkins, E. Haung and C. Qiu, "Working capability analysis of Stewart platforms," *ASME J. Mech. Des.* **118**, 220–227 (1996).
15. J. P. Merlet, "Designing a parallel manipulator for a specific workspace," *Int. J. Robot. Res.* **16**(4), 545–556 (1997).
16. J. Conti, C. Clinton, G. Zhang and A. Wavering, *Workspace Variation of a Hexapod Machine Tool*, NISTIR 6135 (National Institute of Standards and Technology, Gaithersburg, MD, 1998).
17. J. P. Merlet, C. M. Gosselin and N. Mouly, "Workspaces of planar parallel manipulators," *Mech. Mach. Theor.* **33**(1/2), 7–20 (1998).
18. Z. Wang, Z. Wang, W. Liu and Y. Lei, "A study on workspace, boundary workspace analysis and work piece positioning for parallel machine tools," *Mech. Mach. Theor.* **36**, 605–622 (2001).
19. F. Xi, "A comparison study on hexapods with fixed-length legs," *Int. J. Mach. Tools Manu.* **41**, 1735–1748 (2001).
20. M. Badescu and C. Mavroidis, "Workspace optimization of 3-legged UPU and UPS parallel platforms with joint constraints," *ASME J. Mech. Des.* **126**, 291–300 (2004).
21. C. Ferraresi, M. Paoloni and F. Pescarmona, "A new methodology for the determination of the workspace of six-DOF redundant parallel structures actuated by nine wires," *Robotica* **25**, 113–120 (2007).
22. G. Pond and J. A. Carretero, "Quantitative dexterous workspace comparison of parallel manipulators," *Mech. Mach. Theor.* **42**, 1388–1400 (2007).
23. Y. Lu and B. Hu, "Analyzing kinematics and solving active/constrained forces of a 3 SPU+UPR parallel manipulator," *Mech. Mach. Theor.* **42**, 1298–1313 (2007).
24. H. Alp and İ.Özkol, "Extending the workspace of parallel working mechanisms," *J. Mech. Eng. Sci.* **22**, 1305–1313 (2008).
25. D. Glozman and M. Shoham, "Novel 6-dof parallel manipulator with large workspace," *Robotica* **27**, 891–895 (2009).
26. Z. Wang, S. Ji, Y. Li and Y. Wan, "A unified algorithm to determine the reachable and dexterous workspace of parallel manipulators," *Robot. Comput. Integr. Manuf.* **26**, 454–460 (2010).
27. B. Dasgupta and T. S. Mruthyunjaya, "Singularity-free path planning for the Stewart platform manipulator," *Mech. Mach. Theor.* **33**(6), 711–725 (1998).
28. J. P. Merlet, "A generic trajectory verifier for the motion planning of parallel robots," *ASME J. Mech. Des.* **123**, 510–515 (2001).
29. E. Macho, O. Altuzarro, E. Amezua and A. Hernandez, "Obtaining configuration space and singularity maps for parallel manipulators," *Mech. Mach. Theor.* **44**, 2110–2125 (2009).
30. K. Y. Tsai and T. K. Lee, "6-DOF parallel manipulators with better dexterity, rotatibility or singularity-free workspace," *Robotica* **27**, 599–606 (2008).
31. Q. Jiang and C. M.Gosselin, "The maximal singularity-free workspace of the Gough-Stewart platform for a given orientation," *ASME J. Mech. Des.* **130**(11), 112304–112304 (2008).
32. Q. Jiang and C. M. Gosselin, "Determination of the maximal singularity-free orientation workspace for the Gough-Stewart platform," *Mech. Mach. Theor.* **44**, 1281–1293 (2009).
33. J. Enferadi and A. A. Tootoonchi, "A novel spherical parallel manipulator: Forward position problem, singularity analysis, and isotropy design," *Robotica* **27**, 663–676 (2009).
34. Y. Cao, H. Zhou, Q. J. Zhang and W. X. Ji, "Research on the orientation-singularity and orientation-workspace of a class of Stewart-Gough parallel manipulators," *J. Multi-body Dynamics* **224**(K1), 19–32 (2010).
35. C. M. Gosselin and J. Angeles, "The optimum kinematic design of a planar three-degree-of freedom parallel manipulator," *ASME J. Mech. Transmissions Autom. Des.* **110**(1), 35–41 (1988).
36. C. M. Gosselin and J. Angeles, "The optimum kinematic design of a spherical three-degree-of freedom parallel manipulator," *ASME J. Mech. Transmissions Autom. Des.* **111**(2), 202–207 (1989).
37. L. W. Tsai and S. Joshi, "Kinematics and optimization of a spatial 3-UPU parallel manipulator," *ASME J. Mech. Des.* **122**(4), 439–446 (2000).
38. Y. K. Hwang, J. W. Yoon and J. H. Ryu, "The optimum design of a 6-dof parallel manipulator with large orientation workspace," IEEE Int. Conf. Robot. Autom. 163–168, (2007).
39. M. Ruggiu, "Position analysis, workspace and optimization of a 3-PPS spatial manipulator," *ASME J. Mech. Des.* **131**, 051010/1–051010/9 (2009).
40. Y. Wang, C. Wu and X. J. Liu, "Performance evaluation of parallel manipulators: Motion/force transmissibility and its index," *Mech. Mach. Theor.* **45**, 1462–1476 (2010).
41. V. Garg, S. B. Nokleby and J. A. Carretero, "Determining the force and moment workspaces of redundantly-actuated spatial parallel manipulators," *ASME Int. Des. Eng. Tech. Conf. Comp. Inf. Eng. Conf.* **8**, 1063–1070 (2008).
42. B. Güneri, A Complete Dynamic Analysis of Stewart Platform Including Singularity Detection, *M.Sc. Thesis* (İzmir, Turkey: Graduate School of Natural and Applied Sciences, Dokuz Eylül University, 2007).
43. L. W. Tsai, *Robot Analysis: The Mechanics of Serial and Parallel Manipulators* (John Wiley, New York, 1999).
44. O. Masory and J. Wang, "Workspace evaluation of Stewart platforms," *Adv. Rob.* **9**(4), 443–461 (1995).
45. S. Sen, B. Dasgupta and A. K. Mallik, "Variational approach for singularity-free path-planning of parallel manipulators," *Mech. Mach. Theor.* **38**, 1165–1183 (2003).